Available online at www.sciencedirect.com
ScienceDirect
International Journal of Heat and Mass Transfer 50 (2007) 2590–2604
International Journal of HEAT and MASS TRANSFER
www.elsevier.com/locate/ijhmt

Structural optimization of two-dimensional cellular metals cooled by forced convection

T. Wen [a], F. Xu [a], T.J. Lu [a,b,*]

[a] Engineering Department, Cambridge University, Cambridge CB2 1PZ, UK
[b] MOE Key Laboratory of Strength and Vibration, School of Aerospace, Xian Jiaotong University, Xian 710049, PR China

Received 8 September 2006
Available online 24 January 2007

Abstract

We report in this paper analytical results on the optimal design of two-dimensional all metallic sandwiches having lightweight cellular cores subjected to laminar forced convection at fixed pumping power. Various types of core topology are exploited, such as square cells and equilateral triangular cells. The intersection-of-asymptotes method is employed for the optimal design, whilst the fin analogy model is used to account for the contribution of solid conduction. To check the validity and accuracy of the analytical model, the predictions are compared with those obtained using the method of computational fluid dynamics (CFD). The structural parameters of the sandwich optimized include overall length and cell size, with the latter dependent upon porosity and the number of cells along sandwich height. The parameters that may influence the optimally designed sandwich structure are discussed, including overall structural dimensions, pumping power, solid conductivity, and coolant properties.

Keywords: Two-dimensional cellular metals; Laminar forced convection; Optimization; CFD

1. Introduction

Ultra-lightweight cellular metallic materials have attracted increasing interests from academia and industry alike, for their superior mechanical, thermal, acoustic and other physical properties. These novel materials have either random or periodic cellular morphologies and are highly porous, with the porosity level typically exceeding 70% [1]. Examples include aluminum foams and stainless steel lattice block materials. Of particular interest is the understanding and quantification of structure-property relationships for these materials targeting a variety of different applications: structural load bearing, impact energy absorption, heat dissipation, sound attenuation, morphing, etc. [1,2]. Also, those having open channels (flow through topologies) have emerged as excellent candidates for multi-functional applications [2]. Thus, how to obtain the required morphology using multi-objective, multi-parameter optimization techniques becomes a challenge.

Amongst different types of cellular material, the simplest are two-dimensional (2D) arrays of polygons that pack to fill a plane area, often referred to as the 2D cellular materials or honeycombs. All-metallic lightweight sandwich structures with 2D prismatic cores (Fig. 1) have the potential for simultaneous load bearing and active cooling [1]. The load bearing characteristics of these structures have been well-documented in the open literature, demonstrating the structural efficiency benefits of various topologies. Continuous channels of these structural sandwiches allow internal fluid transport, enabling simultaneous active cooling [2]. A comprehensive assessment of these cooling capabilities, involving comparisons between different core topologies, is addressed in this paper. The focus is placed on optimizing the cellular morphology as well as overall sandwich dimensions for maximum thermal performance.

* Corresponding author. Present address: MOE Key Laboratory of Strength and Vibration, School of Aerospace, Xian Jiaotong University, Xian 710049, PR China. Tel.: +86 29 82665600; fax: +86 29 82668234.
E-mail address: tjlu@mail.xjtu.edu.cn (T.J. Lu).

0017-9310/$ - see front matter
doi:10.1016/j.ijheatmasstransfer.2006.11.026

Nomenclature

c_p	specific heat at constant pressure [(kJ/(kg K)]
D_h	cell hydraulic diameter [m]
f	friction factor [–]
$h(z)$	local heat transfer coefficient [W/m^2 K]
$\bar{h}(z)$	overall heat transfer coefficient [W/m^2 K]
H	overall height [m]
k	thermal conductivity [W/(m K)]
l	cell size (shown in Fig. 1) [m]
L	overall length [m]
N	overall cell number ($N = N_H N_W$) [–]
N_H	cell number along the height [–]
N_W	cell number along the width [–]
$Nu(z)$	local Nusselt number [–]
$\overline{Nu}(z)$	overall Nusselt number [–]
P	pumping power [W]
ΔP	pressure drop [Pa]
Pr	Prandtl number [–]
$q''(z)$	local heat flux [W/m^2]
Q	total heat transfer [W]
R	overall thermal resistance [K/W]
Re_{D_h}	Reynolds number based on cell size [–]
Re_z	Reynolds number based on longitudinal position [–]
t	cell wall thickness (shown in Fig. 1) [m]
T	temperature [K]
T_w	constant wall temperature [K]
U	mean coolant velocity in cells [m/s]
U_m	mean coolant velocity upstream [m/s]
W	overall width [m]
x, y, z	Cartesian coordinates (shown in Fig. 2) [–]

Greek symbols

ε	porosity [–]
ϕ	surface area density [1/m]
Ψ	shape factor [–]
μ	dynamic viscosity [kg/(m s)]
ν	kinematic viscosity [m^2/s]
ρ	density [kg/m^3]
$\tilde{\rho}$	relative density [–]
τ	sheer stress [Pa]

Subscripts

f	fluid
in	inlet
s	solid

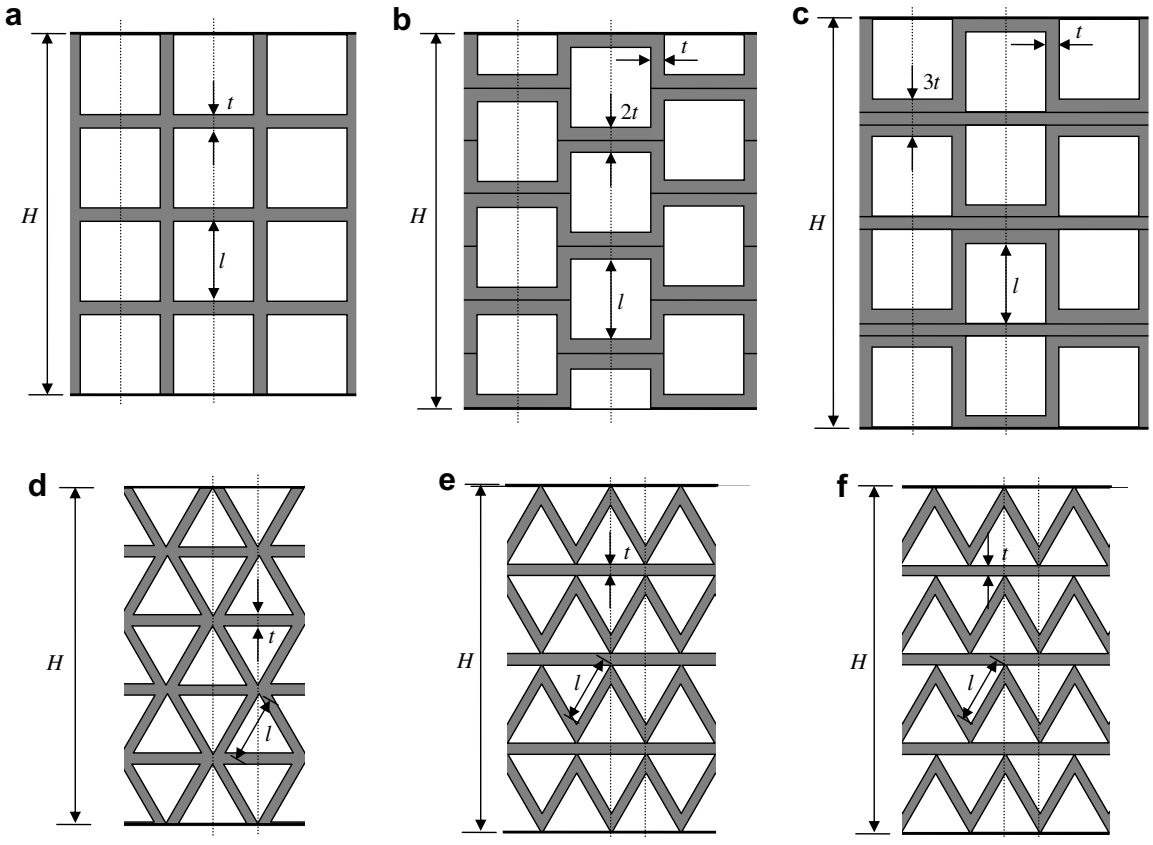

Fig. 1. Different stacking orders for 2D cellular solids having: (a)–(c) rectangular cells; (d)–(f) equilaterally triangular cells.

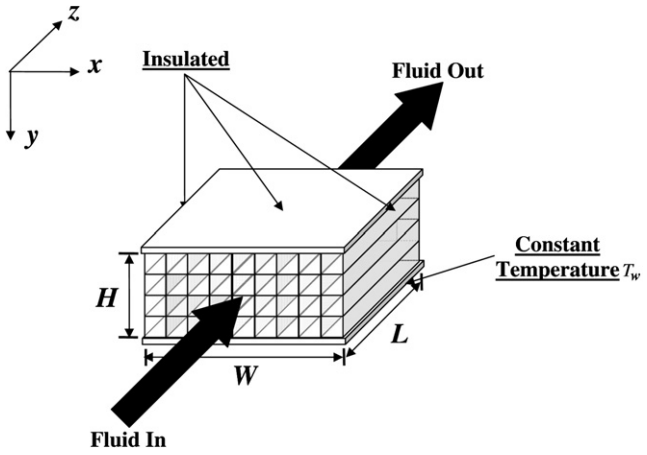

Fig. 2. Schematic of a 2D cellular sandwich heat sink cooled by forced convection; coolant flows along the z-axis.

There is a growing literature on the transport of heat across 2D cellular metallic structures. Using a modified fin analogy model, Lu [3] evaluated the performance of 2D cellular metals with hexagonal cells subjected to forced convection, and obtained the optimal cell morphology for maximum overall heat transfer rate. Built upon this approach, Gu et al. [4] developed analytical models and dimensionless indices that enable simultaneous evaluation of the load bearing and heat dissipation capabilities of 2D cellular metals having square, triangular and hexagonal cells. They employed a two-stage optimization to identify cell morphologies that optimize the structural and heat transfer performance for a specified porosity level. In addition to these analytical approaches, Kumar and McDowell [5] used a finite element method to analyze steady-state convective heat transfer through 2D cellular metals having rectangular cells, and explored the optimized morphology of functionally graded cellular structures. Using the finite difference method for steady-state heat transfer and a multi-objective decision support model, Seepersad et al. [6] designed both periodic and functionally graded 2D cellular structures with desirable structural and thermal attributes.

The works cited above are valuable in exploring the relationship between cellular structure and thermal performance when the overall length of a 2D cellular material/structure is relatively large compared with its cell size, since they only considered the fully developed case whereby the entrance as well as exit effects can be neglected. However, with the increasingly compact requirement of heat sinks designed with 2D cellular metals, developing temperature and flow fields prevail and must be properly accounted for in the design process. In this paper, to address this deficiency, we adopt an intersection-of-asymptotes method to explore the interplay between the structure of a 2D cellular metal and its thermal performance, with the consideration of developing flow/temperature fields an essential feature of our work. This method was first developed by Bejan and Sciubba [7] to optimize the plate spacing for an array of parallel plates cooled by forced convection. Later, Yilmaz et al. [8] applied the method to optimize the shape and dimension of a single duct with constant wall temperature cooled by forced laminar flow. More recently, Muzychka [9] used the method to determine the optimal cell size of 2D cellular metals cooled by forced convection, which is quite close to the current work. However, Muzychka's work is far from solving the problem due to two simplifying assumptions made: (1) cell wall thickness was neglected; as a result, the porosity ε, an important parameter describing any cellular structure, was missed out, and hence the only geometrical parameter that affects the outcome of the optimization is the cell size; (2) thermal conduction resistance in solid walls is neglected; therefore, Muzychka's analysis is restricted to 2D cellular metals having very high solid conductivity.

In the present work, to consider both developing flow effects and thermal conduction in solid walls, we integrate the fin analogy model [3] into the intersection-of-asymptotes method [7]. In addition, the cellular structure of a sandwich heat sink is fully characterized and the effects of various structural parameters on heat sink performance are discussed. The paper is laid out as follows. Section 2 presents the correlations of various topology parameters. In Section 3, the intersection-of-asymptotes method is combined with the fin analogy model to analyze 2D cellular metals. Comparisons between numerical results from CFD (FLUENT™) calculations and the present analytical predictions on both optimal structural parameters and maximum total heat transfer rate are given in Section 4. Section 5 discusses in detail the effects of geometrical parameters, solid conductivity and coolant properties on the optimal structure of 2D cellular metals having either square or equilateral triangular cells.

2. Topology

For a 2D all-metallic sandwich heat sink with periodic cellular core and thin facesheets made of the same metal, besides its overall dimensions ($H \times W \times L$), the following parameters characterize its cross-sectional topology:

(1) Cell shape (square, triangular, etc.).
(2) Stacking order [4], which depends mainly on the fabrication method. Fig. 1 gives different stacking orders for 2D cellular metals having square cells (Fig. 1a–c) and equilateral triangular cells (Fig. 1d–f). Fig. 1a and d can be fabricated using the extrusion technology [10]; Fig. 1b, c, e and f can be fabricated using the crimping and stamping method [11]. Note that Fig. 1a can also be fabricated using the brazing method [12].
(3) Porosity ε, defined as the ratio of void volume to total volume of the cellular material. In the literature, the notion of relative density $\tilde{\rho}$ is often used, which is the density of the cellular material, ρ^*, divided by the density of the solid from which the cell walls are

made, ρ_s. The porosity and relative density are simply related as $\tilde{\rho} = 1 - \varepsilon$.

(4) l/H, which is the ratio between cell size and overall sandwich height; or equivalently, t/H, which is the ratio between cell-wall thickness and overall sandwich height.

For simplicity, the present analysis is restricted to 2D cellular metals with all the cells having uniform wall thickness (Fig. 1a and d). The analysis can nonetheless be extended straightforwardly to cells having double- or even treble-wall thickness, as demonstrated in [3].

For a 2D cellular metal with square cells (Fig. 1a), we have

$$l/H = \frac{1 - (N_H - 1)t/H}{N_H} \tag{1}$$

Correspondingly, the porosity is given by

$$\varepsilon = \frac{N_H (l/H)^2}{l/H + t/H} \tag{2}$$

Similarly, for a 2D cellular metal having equilateral triangular cells (Fig. 1d)

$$l/H = \frac{2}{\sqrt{3}} \frac{1 - (N_H - 1)t/H}{N_H} \tag{3}$$

$$\varepsilon = \frac{\frac{\sqrt{3}}{4} N_H (l/H)^2}{\frac{1}{2} l/H + \frac{2}{\sqrt{3}} t/H} \tag{4}$$

Therefore, for predefined cell shape and stacking order, four geometric parameters defining the cross section: porosity ε, cell number along sandwich height N_H, t/H, and l/H, can be obtained from the above relationships with any two of them given.

3. Analysis

Consider the problem shown in Fig. 2. Coolant, with inlet temperature $T_{f,in}$, is driven by a pumping power P to cool down a 2D cellular-cored sandwich heat sink. One substrate of the sandwich is kept at uniform temperature T_w ($> T_{f,in}$), whilst the other substrate and two sides of the sandwich are thermally insulated. We assume that all cells are subjected to the same pressure drop Δp, which implies that the flow velocities in all the cells are equal. The velocity in each cell, U, is correlated with U_m by

$$U = U_m/\varepsilon \tag{5}$$

The pumping power P needed to drive the coolant through is expressed as

$$P = \Delta p H W U_m \tag{6}$$

By tailoring the cellular structure of the sandwich heat sink, the aim of the optimization is to maximize its total heat transfer rate per unit temperature difference; or, equivalently, to minimize its overall thermal resistance, defined as

$$R = \frac{T_w - T_{f,in}}{Q} \tag{7}$$

where Q is the total amount of heat dissipated.

The analysis described below is analogous to the method employed by Bejan and Sciubba [7].

3.1. Limit I: fully developed case ($D_h \to 0$ or $L \to \infty$)

When each cell is sufficiently slender, the flow is fully developed along L. Meanwhile, the temperatures at the outlet in both the cell wall and fluid are approaching T_w. Therefore, the total heat transfer is

$$Q_I = \rho_f c_p U_m H W (T_w - T_{f,in}) \tag{8}$$

For fully developed flow, the pressure drop in each cell is

$$f Re_{D_h} = 64 \Psi \tag{9}$$

where Ψ is the shape factor, with $\Psi = 0.8875$, and 0.83125 for square and equilateral triangle based on [13], respectively, and

$$f = \frac{\Delta p}{L} D_h \frac{1}{\rho_f U^2/2} \tag{10}$$

$$Re_{D_h} = \frac{U D_h}{\nu_f} \tag{11}$$

Combining Eqs. (6), (9)–(11), we have

$$U = \left(\frac{1}{32\Psi}\right)^{1/2} P^{1/2} \left(\frac{1}{\rho_f \nu_f}\right)^{1/2} \frac{D_h}{\varepsilon^{1/2} H^{1/2} W^{1/2} L^{1/2}} \tag{12}$$

By substituting Eq. (12) into Eq. (8), we can obtain

$$Q_I = \left(\frac{1}{32\Psi}\right)^{1/2} P^{1/2} \frac{\rho_f^{1/2} c_p}{\nu_f^{1/2}} \frac{D_h \varepsilon^{1/2} H^{1/2} W^{1/2}}{L^{1/2}} (T_w - T_{f,in}) \tag{13}$$

Finally, the overall thermal resistance R can be expressed as

$$R_I = \frac{T_w - T_{f,in}}{Q_I} = (32\Psi)^{1/2} \frac{1}{P^{1/2}} \frac{\nu_f^{1/2}}{\rho_f^{1/2} c_p} \frac{L^{1/2}}{D_h \varepsilon^{1/2} H^{1/2} W^{1/2}} \tag{14}$$

3.2. Limit II: boundary layer case ($D_h \to \infty$ or $L \to 0$)

In this case, the boundary layer that lines each surface becomes 'distinct'. The corresponding fluid flow and heat transfer can be approximated by using the theory of boundary layers [13].

For pressure loss

$$\frac{\tau}{\rho_f U^2/2} = 1.328 Re_L^{-1/2} \tag{15}$$

where

$$\tau = \frac{\Delta p}{L}\frac{D_h}{4} \tag{16}$$

$$Re_L = \frac{UL}{v_f} \tag{17}$$

Combining Eqs. (6), (15)–(17), we have

$$U = 0.677P^{2/5}\frac{1}{\rho_f^{2/5}v_f^{1/5}}\frac{D_h^{2/5}}{\varepsilon^{2/5}H^{2/5}W^{2/5}L^{1/5}} \tag{18}$$

For heat transfer in the boundary layer along a flat plate with constant temperature, the local heat transfer coefficient can be calculated by

$$h(z) = Nu(z)\frac{k_f}{z} = 0.332\frac{k_f}{z}Pr^{1/3}Re_z^{1/2} \tag{19}$$

The overall heat transfer coefficient averaged from $z = 0$ to z corresponding to the local heat transfer coefficient Eq. (19) is

$$\bar{h}(z) = \frac{1}{z}\int_0^z h(z)\mathrm{d}z = 0.664\frac{k_f}{z}Pr^{1/3}Re_z^{1/2} \tag{20}$$

For heat transfer in the boundary layer along a flat plate with arbitrary temperature distribution $T_w(z)$, the local heat flux can be calculated by

$$q''(z) = h(z)\int_0^z \frac{\mathrm{d}T_w(\eta)/\mathrm{d}\eta}{[1-(\eta/z)^{3/4}]^{1/3}}\mathrm{d}\eta + h(z)[T_w(0) - T_{f,in}] \tag{21}$$

3.2.1. Thermal conduction resistance in cell walls ignored ($k_s \to \infty$)

When the conduction resistance in cell walls is neglected ($k_s \to \infty$), the walls are isothermal with temperature T_w, and the total heat transfer rate can be calculated as

$$Q_{II} = \bar{h}_L NCL(T_w - T_{f,in}) \tag{22}$$

where $\bar{h}_L$ is the overall heat transfer coefficient averaged from $z = 0$ to L calculated by Eq. (20); N is the overall cell number; and C is the perimeter of each cell. Consequently, the total heat transfer is

$$Q_{II} = 0.546P^{1/5}\frac{k_f Pr^{1/3}}{\rho_f^{1/5}v_f^{3/5}}\frac{D_h^{1/5}L^{2/5}NC}{\varepsilon^{1/5}H^{1/5}W^{1/5}}(T_w - T_{f,in}) \tag{23}$$

Correspondingly, the overall thermal resistance is

$$R_{II} = \frac{T_w - T_{f,in}}{Q_{II}} = 1.832\frac{1}{P^{1/5}}\frac{\rho_f^{1/5}v_f^{3/5}}{k_f Pr^{1/3}}\frac{\varepsilon^{1/5}H^{1/5}W^{1/5}}{D_h^{1/5}L^{2/5}NC} \tag{24}$$

3.2.2. Thermal conduction resistance in cell walls included (finite k_s)

To address the effects of thermal conduction resistance in solid walls, we adopt the popular fin analogy model [3,4]. With the periodic unit of the cellular structure modeled as a corrugated wall with fins, a two-step analysis is employed: the transfer of heat across a corrugated wall without fins is analyzed first; the contribution of the fins is subsequently included separately (Fig. 3).

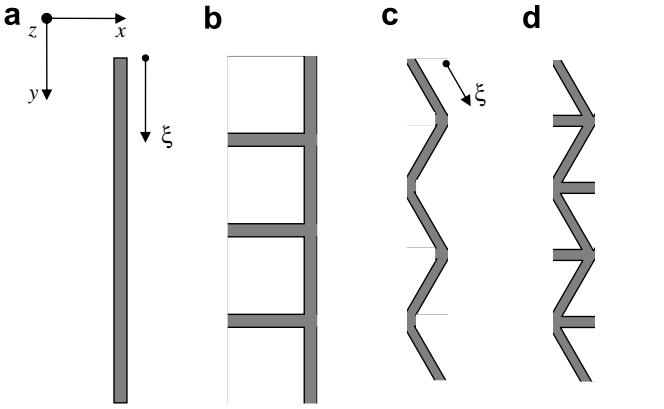

Fig. 3. Two-step analysis in fin analogy model: (a) and (c) single-corrugated walls without fins for square and triangular shaped cells; (b) and (d) corrugated walls with fin attachments for square and triangular shaped cells; local coordinate is ξ.

Heat transfer along a single-corrugated wall without fins at axial position z is a one-dimensional conduction problem, with the convective heat by the coolant modeled as a source term. With Eq. (21), the variation of temperature $T_s(\xi, z)$ along the length of a single-corrugated wall is governed by

$$k_s t\frac{\partial^2 T_s(\xi,z)}{\partial\xi^2} - 2h(z)\left[\int_0^z \frac{\partial T_s(\xi,\eta)/\partial\eta}{\left[1-(\eta/z)^{3/4}\right]^{1/3}}\mathrm{d}\eta + T_s(\xi,0) - T_{f,in}\right] = 0 \tag{25}$$

Here, $h(z)$ is the local heat transfer coefficient given by Eq. (19), and ξ is the local coordinate along the corrugated wall (Fig. 3), with

$$\begin{cases} \xi = 0, & y = 0, \\ \xi = c_H H, & y = H \end{cases} \tag{26}$$

where c_H is the tortuous coefficient: $c_H = 1.0$, and 1.155 for square and equilateral triangle, respectively [4].

The boundary conditions are

$$\begin{cases} k_s\frac{\partial T_s}{\partial\xi} = 0, & \xi = 0, \\ T_s = T_w, & \xi = c_H H \end{cases} \tag{27}$$

Eq. (25) is an integro-differential equation, which is rather difficult to deal with. For simplicity, we replace $\int_0^z \frac{\partial T_s(\xi,\eta)/\partial\eta}{[1-(\eta/z)^{3/4}]^{1/3}}\mathrm{d}\eta + T_s(\xi,0)$ by $T_s(\xi,z)$ so that Eq. (25) can be simplified as

$$k_s t\frac{\partial^2 T_s(\xi,z)}{\partial\xi^2} - 2h(z)[T_s(\xi,z) - T_{f,in}] = 0 \tag{28}$$

To estimate the feasibility of the above approximation, the second terms on the left hand sides of Eqs. (25) and (28), which represent separately the accurate and estimated local convective heat flux q'', are compared in Fig. 4. The cell

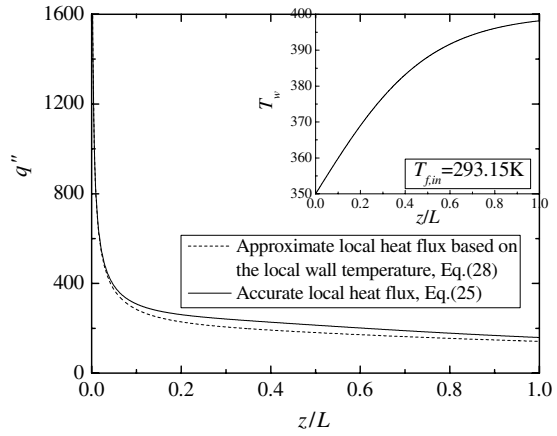

Fig. 4. Local heat flux calculated by replacing $T_s(\xi,0)+\int_0^{\xi}\frac{\partial T_s(\xi,\eta)/\partial\eta}{[1-(\eta/z)^{3/4}]^{1/3}}d\eta$ in Eq. (25) with $T_s(\xi,z)$ in Eq. (28). Wall temperature is chosen as a TANH profile similar to the temperature distribution obtained directly by CFD calculation.

wall temperature $T_s(\xi,z)$, when $\xi \neq c_H H$, is chosen as a TANH profile along z, mimicking that calculated by using the commercially available CFD code, FLUENT™ [12]. The results of Fig. 4 demonstrate that the simplification leads to approximately 10% underestimation in the local convective heat transfer, which is considered acceptable.

The solution to Eq. (28) with boundary conditions Eq. (27) is given by

$$T_s(\xi,z)=T_{f,in}+(T_w-T_{f,in})\frac{\cosh\left(\sqrt{2h(z)/k_s t}\,\xi\right)}{\cosh\left(\sqrt{2h(z)/k_s t}\,c_H H\right)} \tag{29}$$

The total amount of heat dissipated to the coolant per unit length of the corrugated wall is

$$q_1(z)=k_s t\left.\frac{dT_s}{d\xi}\right|_{\xi=c_H H} =(T_w-T_{f,in})\sqrt{2h(z)k_s t}\tanh\left(\sqrt{2h(z)/(k_s t)}\,c_H H\right) \tag{30}$$

Solving for the exact solution of additional heat loss from the fins is quite complicated. By introducing a parameter c_{fin}, which denotes the weight coefficient of fins on total heat loss, an approximate solution considering the contribution of fins can be obtained, which provides a good approximation for the exact solution [3], as

$$q(z)=(1+c_{fin})(T_w-T_{f,in})\sqrt{2h(z)k_s t}\tanh\left(\sqrt{2h(z)/(k_s t)}\,c_H H\right) \tag{31}$$

The weight coefficient c_{fin} can be estimated by the surface area ratio of fins to corrugated wall.

Finally, the total heat transfer rate from the heat sink can be calculated by

$$Q_{II}=\int_0^L [N_w q(z)+q_w(z)]dz \tag{32}$$

where $q_w(z)$ is the heat flux into the coolant from the remaining surface of the heated substrate, given by

$$q_w(z)=h(z)(W-N_w c_H t)(T_w-T_{f,in}) \tag{33}$$

Therefore, in the limit $D_h\to\infty$, the total heat transfer can be obtained by combining Eqs. (31)–(33). The corresponding overall thermal resistance is given by

$$R_{II}=\frac{T_w-T_{f,in}}{Q_{II}}=\frac{T_w-T_{f,in}}{\int_0^L[N_w q(z)+q_w(z)]dz} \tag{34}$$

3.3. Intersection of the two asymptotes

In the limit I, when $D_h\to 0$ (or $L\to\infty$), from Eq. (14), we have

$$\frac{T_w-T_{f,in}}{Q_I}\sim\frac{L^{1/2}}{D_h} \tag{35}$$

This means that for fully developed flow, the overall thermal resistance of the heat sink decreases with D_h^{-1} for a finite L [line (a) in Fig. 5a] or increases with $L^{1/2}$ for a finite D_h [line (a) in Fig. 5b].

For the limit II, when $D_h\to\infty$ (or $L\to 0$), results from Eq. (34) are asymptotic to those from Eq. (24) when the

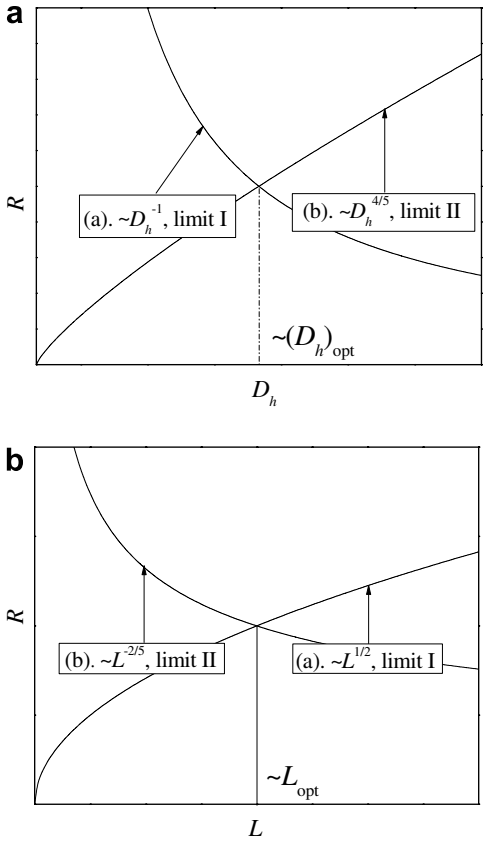

Fig. 5. Method of intersecting asymptotes: (a) cell size as free parameter; (b) heat sink length as free parameter.

solid conductivity tends to be infinity. With Eq. (24), as $N \sim HW\varepsilon/D_h^2$ and $C \sim D_h$, we have

$$\frac{T_w - T_{f,in}}{Q_{II}} \sim \frac{D_h^{4/5}}{L^{2/5}} \tag{36}$$

which implies that for boundary layer flow, the overall thermal resistance increases with $D_h^{4/5}$ for a finite L [line (b) in Fig. 5a] or decreases with $L^{-2/5}$ for a finite D_h [line (b) in Fig. 5b].

Therefore, D_h (or L) can be optimized by intersecting Eq. (14) with either Eq. (24) (for $k_s \to \infty$) or Eq. (34) (for low to medium k_s). Since D_h is correlated with ε and N_H, the latter is used in lieu of D_h in the analysis below. From Eqs. (14), (24) and (34), it is found that the optimal L, ε, N_H and the overall thermal resistance are influenced by the following parameters: (1) overall dimensions; (2) pumping power P; (3) solid conductivity k_s; (4) coolant properties.

There are generally three flow configurations in different applications for a heat sink, which are fixed pumping power, fixed pressure drop and fixed flow rate, depending on how the heat sink is attached to the coolant network [14]. In the above analysis, we particularly address the situation where the pumping power is fixed. This method can nevertheless be extended to the other two situations by replacing the correlations between velocity U and pumping power P [Eqs. (12) and (18)] with those between U and pressure drop or flow rate, respectively (see [14] for detail).

4. Validation of the model

To examine the validity and accuracy of the solutions obtained using the above analytical model, numerical results obtained with FLUENT™ are used for comparison. In the numerical calculations, the periodic unit was chosen as the calculation domain, with a flow developing channel before the sample included to make sure the flow across the core can approximate the condition of a fixed pressure drop. The boundary conditions are similar to those used in our previous paper [12] and are described as follows:

(1) A velocity-inlet boundary condition with a uniform value was assumed at the entrance of the inlet channel; and a pressure-outlet boundary condition with zero gauge pressure was employed at the exit of the sample cell duct.
(2) A constant heat flux boundary condition was employed at the bottom face-sheet of the sample, while the top and bottom walls of the flow developing channel as well as the top face-sheet of the sample were insulated.
(3) Symmetrical boundary conditions for all side surfaces of the sample in the sample's width direction were employed.
(4) The inner surfaces of each cell were set as coupled thermal conditions so that the heat exchange between adjacent zones, belonging to the solid region and the fluid region, respectively, can be calculated. In the fluid side of these inner surfaces, non-slip boundary condition was employed.
(5) A zero-shear boundary condition was employed at the inner surface of the flow developing channel so that the inclusion of the flow developing channel does not affect the uniformity of velocity distribution upstream the inlet of the sample.

It is difficult to obtain the optimal cell size numerically as it is highly expensive to generate the geometries and grids of different cross-sectional topologies. However, because it is relatively straightforward to change sample length, the optimal length calculated from the two methods will be compared below. The cross-sectional topology considered in the numerical simulation is a 2D cellular sandwich structure of height $H = 0.012$ m, width $W = 5H$ and porosity 0.9; in addition, there are in total 6 identical square cells arranged along the channel height (or, equivalently, $t = 0.12$ mm and $l = 1.9$ mm). The solid conductivity is chosen as that of copper: $k_s = 401$ W/m K. At the inlet, the velocity of fluid (air) varies from 2 to 12 m/s, with increasing step size of 0.25 m/s.

For a finite pumping power, coolant velocity varies with increasing overall length and, correspondingly, the overall thermal resistance also changes, as shown in Fig. 6a. As it is computationally impossible to obtain continuous variation of overall length, the exact value of L/H minimizing the overall thermal resistance cannot be determined numerically. However, a finite range of L/H, within which the overall thermal resistance may achieve its minimum, can be obtained. For different pumping powers, the numerically determined optimal values of L/H are compared in Fig. 6b with those predicted by the intersection-of-asymptotes method. In Fig. 6c, the corresponding values of minimum overall thermal resistance from CFD calculations and intersection-of-asymptotes method are compared.

From Fig. 6b it is seen that all the predictions for optimal overall length fall into the CFD determined range, thus demonstrating the feasibility of the present method in predicting the optimal geometries.

The results of Fig. 6c show that the predicted values of minimum overall thermal resistance are nearly half those of the CFD results. This is to be expected, for two reasons. Firstly, in the fully developed flow limit, the assumption that both the fluid and wall temperatures approach T_w is valid when the duct is sufficiently long (much longer than the present optimized length); furthermore, the lower the solid conductivity, the longer the duct. Secondly, in the developing flow limit, the boundary layers along joint walls merge at the corner and, as the thickness of the boundary layer grows in the longitudinal direction, the boundary layers along opposite walls also merge. This

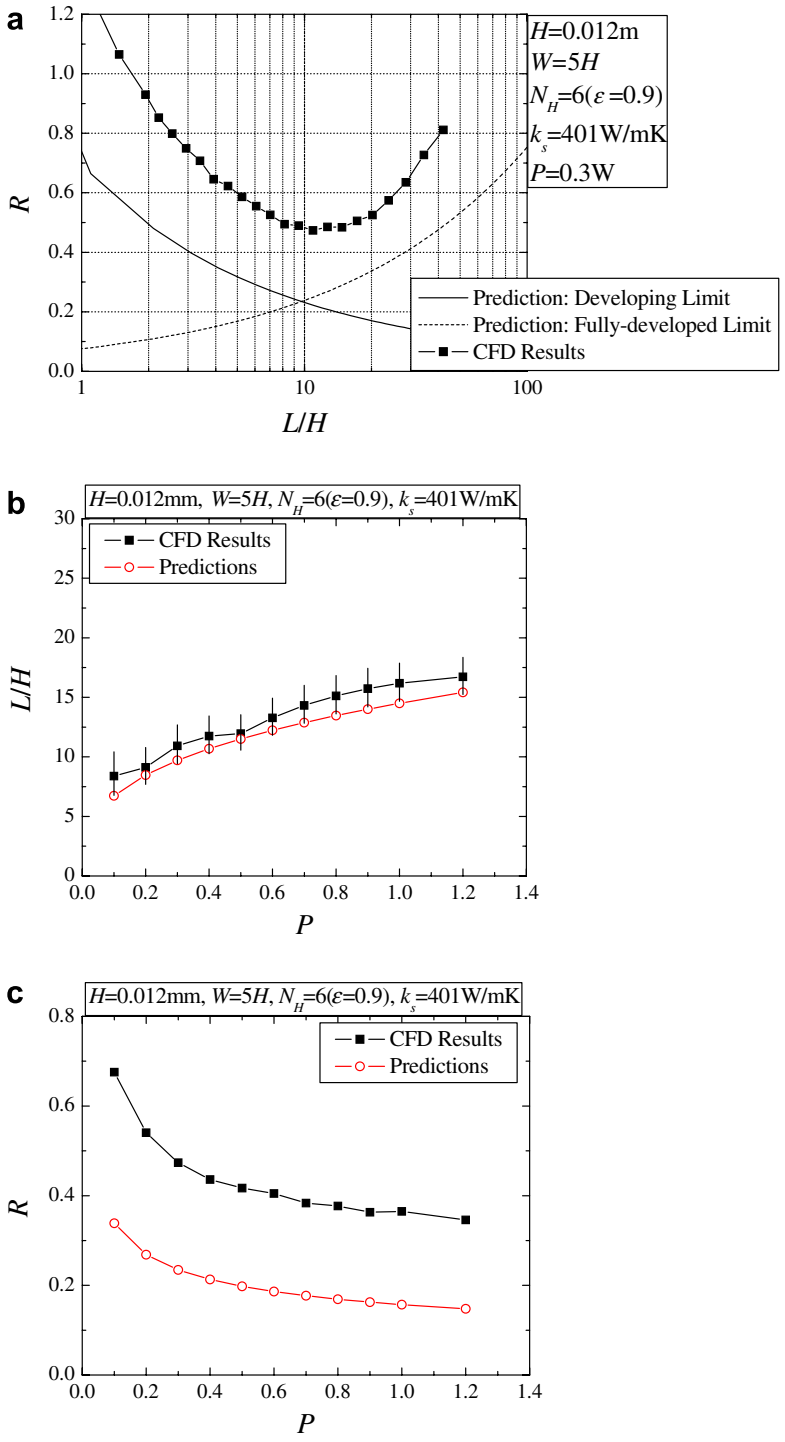

Fig. 6. Comparisons between results from CFD (FLUENT™) calculations and model predictions: (a) pumping power fixed at $P = 0.3$ W, with $H = 0.012$ m, $W = 5H$, $N_H = 6$ and $k_s = 401$ W/m K; (b) optimum L/H and (c) minimum overall thermal resistance for different pumping powers.

suggests that the flow in the developing section of each cell duct is not simply the summation of boundary layers along each wall as simplified in the intersection-of-asymptote method.

Although the model somewhat underestimates the overall thermal resistance, the predictions are qualitatively accordant with CFD calculations, thus do not affect the predictions on optimal structural parameters.

5. Results and discussion

5.1. Optimal overall length

In this section, the optimal overall length of a 2D cellular sandwich heat sink with square cells shown in Fig. 1a is discussed. The coolant considered is air (properties given in Table 1).

Table 1
Fluid properties

Parameters	Unit	Air	Water
Density, ρ_f	kg/m^3	1.225	998.2
Dynamic viscosity, μ_f	kg/(m s)	1.7894×10^{-5}	0.001003
Kinematic viscosity, v_f	m^2/s	1.4607×10^{-5}	1.0048×10^{-6}
Specific heat at constant pressure, c_p	J/(kg K)	1006.43	4182
Fluid thermal conductivity, k_f	W/(m K)	0.0242	0.6
Thermal diffusivity, α_f	m^2/s	1.963×10^{-5}	1.4373×10^{-7}
Prandtl number, Pr	–	0.7441	6.99

Firstly, with the cross-sectional dimensions ($H = 0.012$ m, $W = 5H$) and pumping power ($P = 0.5$ W) prespecified, the variation of optimal L/H and the corresponding overall thermal resistance with different cross-sectional topologies and different solid conductivities are presented in Fig. 7, with Fig. 7a–e corresponding to $k_s = 1$, 10, 100, 1000 W/m K and infinity, respectively.

The results of Fig. 7 demonstrate that, for a 2D cellular structure with fixed cross-sectional topologies (fixed ε and N_H), the optimal L decreases with increasing k_s; for a cellular structure with fixed k_s, the optimal L increases with increasing cell size (decreasing N_H for a finite ε, or increasing ε with N_H fixed).

The variation of overall thermal resistance with different k_s and different cross-sectional topologies is quite complicated. Generally, for a 2D cellular structure with certain cross-sectional topology, the enhancement of k_s decreases the overall thermal resistance. In low k_s regimes (Fig. 7a and b), when ε is fixed, the overall thermal resistance increases as N_H is increased. In medium k_s regions (Fig. 7c and d), for a fixed ε, the overall thermal resistance first slightly decreases, then increases as N_H is increased; in other words, there exists an optimal N_H. The optimal N_H increases with k_s and, for a finite k_s, the optimal N_H decreases with increasing ε. In the ideal limit that $k_s \to \infty$ (Fig. 7e), the overall thermal resistance decreases slightly with N_H. Again, from Fig. 7a–e, we can find that when N_H is fixed, there also exists an optimal ε in low and medium k_s regimes, which increases with increasing k_s and for a finite k_s, increases with decreasing N_H.

The phenomena observed in Fig. 7a–e clearly demonstrate the role of coupled conduction–convection mechanism in the process of heat dissipation across 2D cellular structures, as elucidated below.

From Fourier's law of conduction, the conduction process is related to cell-wall thickness t and solid conductivity k_s. Increasing either t or k_s enables more heat to be conducted. The cell-wall thickness t is a function of N_H and ε: either increasing N_H with ε unchanged or increasing ε with N_H unchanged will reduce t.

On the other hand, from Newton's law of cooling, the convection process is related to the surface area density ϕ of the structure and the convective heat transfer coefficient $\bar{h}$. Enhancing either ϕ or $\bar{h}$ enables more heat to be convected. The surface area density ϕ is a geometric parameter that depends uponN_H and ε: either increasing N_H with ε unchanged or increasing ε with N_H unchanged will increase ϕ. The convective heat transfer coefficient $\bar{h}$, for laminar duct flow, depends on different thermal boundary conditions and the non-dimensional longitudinal position of the duct exit, $L^* = L/(D_h Re_{D_h} Pr)$. Mathematically, the relationship is highly complicated [13], which is the reason why we adopt the intersection-of-asymptotes method in this paper. For further discussion, the following important conclusions for convective heat transfer in laminar duct flow are noted: (1) for a certain thermal boundary condition, $\bar{h}$ decreases with the increase of L^*; (2) uniform heat flux and isothermal walls are separately the high and low limit cases in overall convective heat transfer coefficient of the more general thermal boundary conditions.

It has been established that an increase in convection by increasing ϕ leads to a decrease in conduction as t is necessarily decreased, which indicates that there exists a balance between convection and conduction processes. From the thermal resistance point of view, reducing the largest thermal resistance will dramatically enhance the overall heat transfer. In other words, the optimal N_H and optimal ε observed in Fig. 7 happen when the convective and conductive resistances are comparative. Both increase with increasing k_s as this reduces the conductive resistance (with the increase of k_s, although the optimal L decreases, which contributes to a decrease in convective resistance due to a decrease in L^* and consequently an increase in $\bar{h}$, this decrement is relatively small compared to the decrease in conductive resistance). For a finite k_s, the increase in ε for a finite N_H leads to higher ϕ and higher $\bar{h}$ (smaller L^*), causing a decrease in convective resistance; the conductive resistance needs to be reduced correspondingly by increasing t to make the convective and conductive resistances comparative. Consequently, the optimal N_H decreases as ε is increased. Similarly, the decrease of N_H for a finite ε leads to a decrease in conductive resistance, so that the convective resistance needs to be reduced by increasing either $\bar{h}$ or ϕ. Although $\bar{h}$ increases with decreasing N_H (smaller L^*), the decrease in convective resistance due to increase in $\bar{h}$ is relatively small in comparison with the decrease in conductive resistance (due to increase in t), requiring therefore a higher ϕ. As a result, the optimal ε increases as N_H is decreased.

With $H = 0.012$ m and $P = 0.5$ W fixed, the variation of optimal L/H and the corresponding overall thermal resistance with different values of channel width W are given

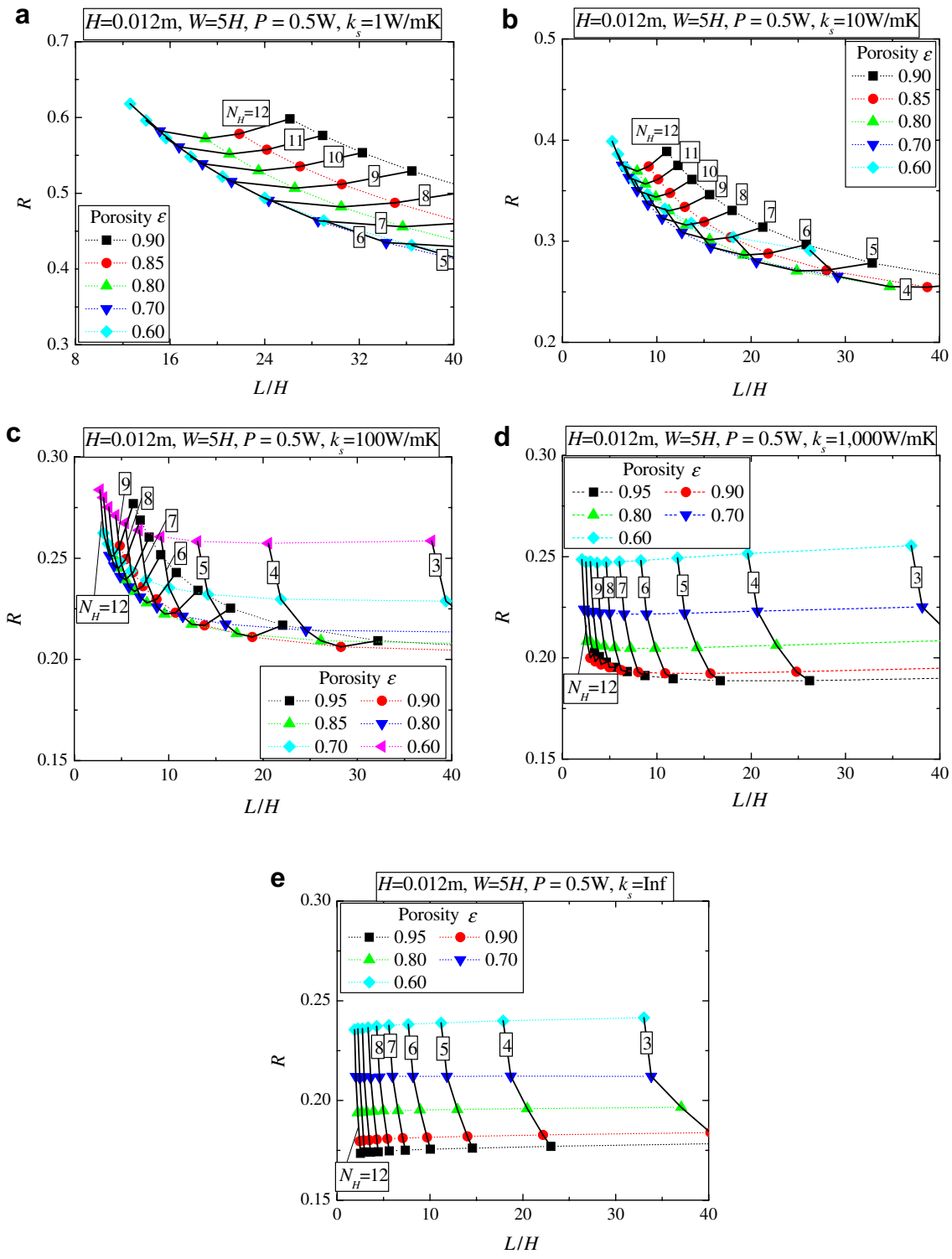

Fig. 7. Optimum heat sink length L/H and corresponding overall thermal resistance for square cells and selected values of porosity ε and cell number N_H, with $H = 0.012$ m, $W = 5H$, $P = 0.5$ W and: (a) $k_s = 1$ W/m K; (b) $k_s = 10$ W/m K; (c) $k_s = 100$ W/m K; (d) $k_s = 1000$ W/m K; (e) $k_s \to \infty$; the working fluid is air ($Pr = 0.74$).

in Table 2. Here, $N_H = 6$, ε varies between 0.50 and 0.95, and k_s is chosen as 100 W/m K. Generally, when ε is fixed, both the optimal L/H and the overall thermal resistance decrease as W is increased. On the other hand, W does not influence optimal ε.

Table 3 gives the variation of optimal L/H and corresponding overall thermal resistance with different cross-sectional dimensions, with the aspect ratio fixed at $W = 5H$ and the pumping power at $P = 0.5$ W. Again, $N_H = 6$, ε varies between 0.50 and 0.95, and $k_s = 100$ W/m K.

Table 2
Optimum heat sink length L/H and corresponding overall thermal resistance for square cells and selected values of heat sink width W and porosity ε, with $H = 0.012$ m, $N_H = 6$, $P = 10$ W and $k_s = 100$ W/m K; the working fluid is air ($Pr = 0.74$)

	$W/H = 1$		$W/H = 3$		$W/H = 5$		$W/H = 7$		$W/H = 9$	
	$(L/H)_{opt}$	R	$(L/H)_{opt}$	R	$(L/H)_{opt}$	R	$(L/H)_{opt}$	R	$(L/H)_{opt}$	R
$\varepsilon = 0.50$	15.26	0.897	9.37	0.406	7.99	0.290	7.18	0.232	6.51	0.195
$\varepsilon = 0.55$	16.38	0.848	10.04	0.383	8.58	0.274	7.53	0.217	6.96	0.184
$\varepsilon = 0.60$	17.50	0.806	10.74	0.364	9.16	0.261	8.03	0.206	7.46	0.175
$\varepsilon = 0.65$	18.66	0.770	11.45	0.348	9.77	0.249	8.57	0.197	7.80	0.166
$\varepsilon = 0.70$	19.87	0.740	12.20	0.335	10.05	0.235	9.12	0.189	8.31	0.159
$\varepsilon = 0.75$	21.18	0.715	13.01	0.324	10.73	0.228	9.74	0.183	8.86	0.154
$\varepsilon = 0.80$	22.67	0.695	13.94	0.315	11.50	0.221	10.18	0.176	9.50	0.150
$\varepsilon = 0.85$	24.49	0.682	15.08	0.309	12.45	0.217	11.02	0.173	10.09	0.146
$\varepsilon = 0.90$	27.09	**0.680**	16.74	**0.308**	13.82	**0.216**	12.24	**0.172**	11.20	**0.145**
$\varepsilon = 0.95$	32.26	0.704	20.02	0.320	16.55	0.225	14.67	0.179	13.43	0.151

Table 3
Optimum heat sink length L/H and corresponding overall thermal resistance for square cells and selected values of heat sink height H and porosity ε, with $W = 5H$, $N_H = 6$, $P = 10$ W and $k_s = 100$ W/m K; the working fluid is air ($Pr = 0.74$)

	$H = 0.008$ m		$H = 0.012$ m		$H = 0.020$ m		$H = 0.050$ m		$H = 0.100$ m	
	$(L/H)_{opt}$	R	$(L/H)_{opt}$	R	$(L/H)_{opt}$	R	$(L/H)_{opt}$	R	$(L/H)_{opt}$	R
$\varepsilon = 0.50$	6.98	0.499	7.99	0.290	9.48	0.147	12.85	0.0433	16.19	0.0172
$\varepsilon = 0.55$	7.50	0.471	8.58	0.274	10.16	0.139	13.79	0.0409	17.38	0.0162
$\varepsilon = 0.60$	8.00	0.448	9.16	0.261	10.86	0.132	14.74	0.0389	18.57	0.0154
$\varepsilon = 0.65$	8.54	0.428	9.77	0.249	11.59	0.126	15.72	0.0372	19.80	0.0148
$\varepsilon = 0.70$	8.79	0.404	10.05	0.235	11.92	0.119	16.18	0.0351	20.39	0.0139
$\varepsilon = 0.75$	9.38	0.391	10.73	0.228	12.72	0.115	17.26	0.0339	21.75	0.0135
$\varepsilon = 0.80$	10.04	0.380	11.50	0.221	13.63	0.112	18.50	0.0330	23.30	0.0131
$\varepsilon = 0.85$	10.88	0.373	12.45	0.217	14.76	0.110	20.02	0.0324	25.23	0.0129
$\varepsilon = 0.90$	12.07	**0.372**	13.82	**0.216**	16.38	**0.109**	22.23	**0.0323**	28.00	**0.0128**
$\varepsilon = 0.95$	14.46	0.387	16.55	0.225	18.62	0.114	27.15	0.0340	33.55	0.0133

The results demonstrate that, with ε fixed, the optimal L/H increases as the overall cross-sectional dimensions increase, whilst the overall thermal resistance decreases with increasing the overall cross-sectional dimensions. Again, the optimal ε is not affected by various cross-sectional dimensions.

Finally, the dependence of optimal L/H and corresponding overall thermal resistance upon pumping power is given in Table 4. The cross-sectional dimensions ($H = 0.012$ m, $W = 5H$) are fixed; $N_H = 6$, ε varies between 0.50 and 0.95, and $k_s = 100$ W/m K. It is found that, when ε is fixed and P is increased, the optimal L/H increases and the overall thermal resistance decreases. Once again, the optimal ε does not depend on P.

5.2. Optimal cell number along sandwich height

In this section, the optimal cell number N_H along the height of a cellular sandwich having square cells (Fig. 1a) is discussed. Again, the coolant considered is air.

Table 4
Optimum heat sink length L/H and minimum thermal resistance for square cells and selected values of pumping power and porosity ε, with $H = 0.012$ m, $W = 5H$, $N_H = 6$ and $k_s = 100$ W/m K; the working fluid is air ($Pr = 0.74$)

	$P = 0.1$ W		$P = 0.2$ W		$P = 0.5$ W		$P = 1.0$ W		$P = 2.0$ W		$P = 5.0$ W	
	$(L/H)_{opt}$	R	$(L/H)_{opt}$	R	$(L/H)_{opt}$	R	$(L/H)_{opt}$	R	$(L/H)_{opt}$	R	$(L/H)_{opt}$	R
$\varepsilon = 0.50$	4.70	0.496	5.89	0.394	7.99	0.290	10.06	0.230	12.68	0.183	17.21	0.135
$\varepsilon = 0.55$	5.01	0.469	6.33	0.372	8.58	0.274	10.80	0.218	13.61	0.173	18.46	0.127
$\varepsilon = 0.60$	5.38	0.446	6.76	0.354	9.16	0.261	11.55	0.207	14.54	0.164	19.73	0.121
$\varepsilon = 0.65$	5.73	0.426	7.21	0.338	9.77	0.249	12.31	0.198	15.51	0.157	21.04	0.116
$\varepsilon = 0.70$	5.89	0.402	7.42	0.319	10.05	0.235	12.67	0.187	15.96	0.148	21.66	0.109
$\varepsilon = 0.75$	6.29	0.389	7.91	0.309	10.73	0.228	13.52	0.181	17.02	0.143	23.11	0.106
$\varepsilon = 0.80$	6.74	0.379	8.48	0.300	11.50	0.221	14.49	0.176	18.25	0.140	24.76	0.103
$\varepsilon = 0.85$	7.29	0.372	9.18	0.295	12.45	0.217	15.68	0.173	19.76	0.137	26.81	0.101
$\varepsilon = 0.90$	8.08	**0.371**	10.18	**0.294**	13.82	**0.216**	17.41	**0.172**	21.92	**0.136**	29.76	**0.100**
$\varepsilon = 0.95$	9.69	0.385	12.20	0.306	16.55	0.225	20.85	0.179	26.27	0.142	35.65	0.105

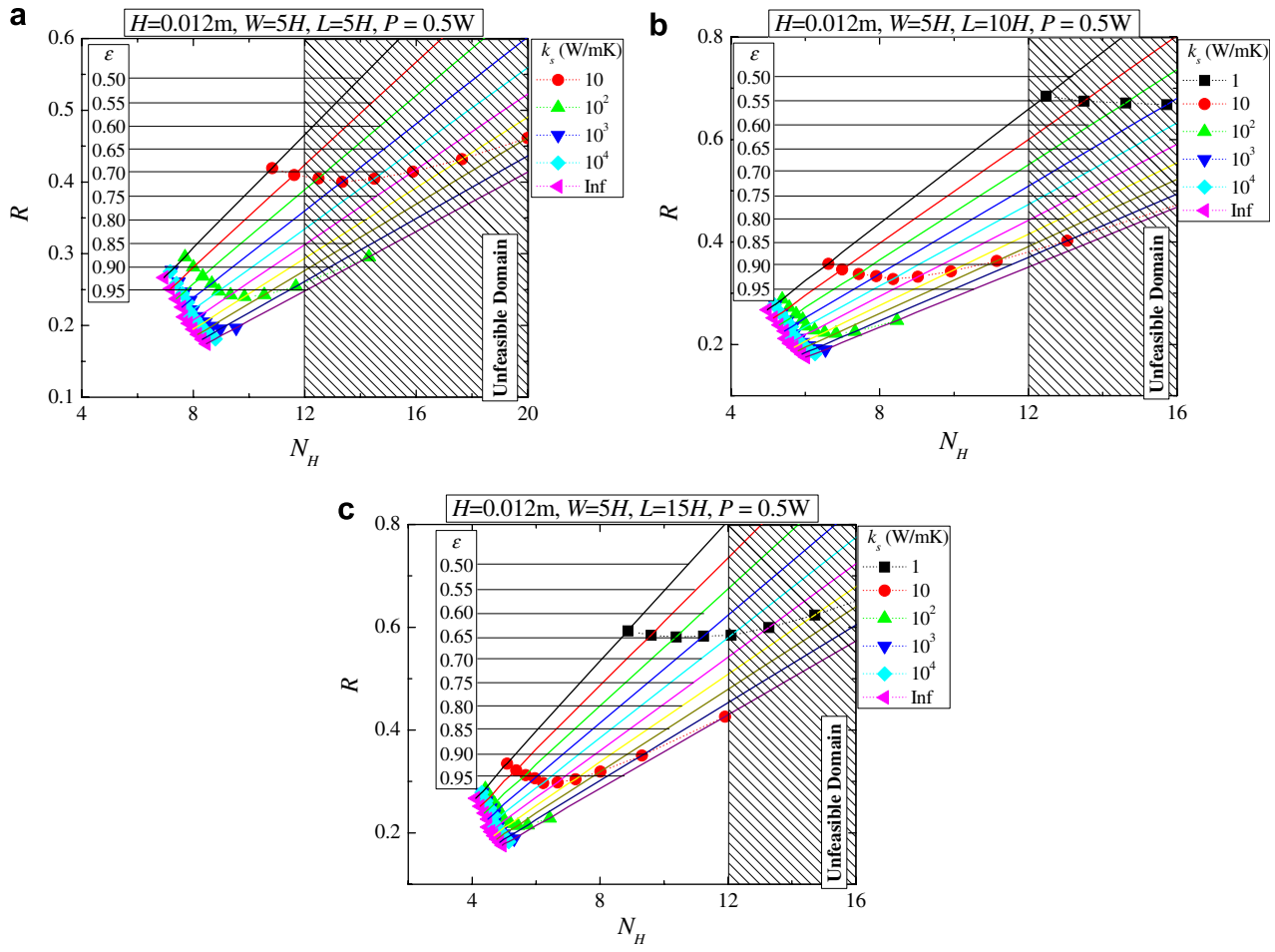

Fig. 8. Optimum cell number N_H and corresponding overall thermal resistance for square cells and selected values of porosity ε and solid conductivity k_s, with $H = 0.012$ m, $W = 5H$, $P = 0.5$ W and: (a) $L = 5H$; (b) $L = 10H$; (c) $L = 15H$; the working fluid is air ($Pr = 0.74$).

In Fig. 8, with the overall dimensions ($H = 0.012$ m, $W = 5H$ and $L = 5H, 10H$ or $15H$) and pumping power ($P = 0.5$ W) predefined, the variations of optimal N_H and the corresponding overall thermal resistance with different selections of ε and k_s are presented. Note that when N_H is larger than 12 for $H = 0.012$ m, the cell size drops below 1.0 mm, making the fabrication of the cellular material using traditional processing technology impractical. In this case, the above model is assumed to be no longer feasible; the corresponding domains are marked as 'unfeasible domain'.

Fig. 8 demonstrates that both the optimal N_H and the overall thermal resistance decrease as k_s increases. When k_s is larger than 1000 W/m K, both the optimal N_H and overall thermal resistance approach those corresponding to the limit $k_s \to \infty$. This implies that, with the fin analogy model included, the analysis of Section 3.2.2 covers that of Section 3.2.1 as a special case. In small and medium k_s ranges (up to 1000 W/m K), an optimal ε exists, which increases with k_s when L is fixed; on the other hand, for a finite k_s, the optimal ε increases slightly with L. This, once again, highlights the important role of coupled conduction–convection mechanism (see Section 5.1).

With both the overall height and length of the sandwich ($H = 0.012$ m, $L = 10H$) and the pumping power ($P =$

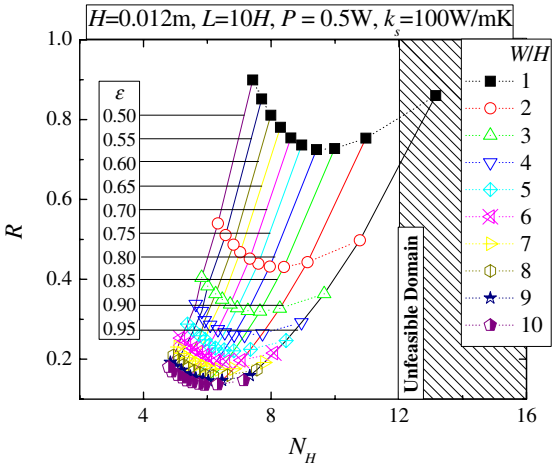

Fig. 9. Optimum cell number N_H and corresponding overall thermal resistance for square cells and selected values of heat sink width W and porosity ε, with $H = 0.012$ m, $L = 10H$, $P = 0.5$ W and $k_s = 100$ W/m K; the working fluid is air ($Pr = 0.74$).

0.5 W) fixed, the variation of optimal N_H and corresponding overall thermal resistance with different selections of sandwich width W are shown in Fig. 9. Here, ε varies between 0.50 and 0.95, and $k_s = 100$ W/m K. Generally, with ε fixed, both the optimal N_H and the overall thermal resistance decreases with increasing W. With the ratios $W/H = 5$ and $L/H = 10$ fixed and pumping power $P = 0.5$ W, Fig. 10 shows the dependence of optimal N_H and corresponding overall thermal resistance on sandwich height H. The optimal N_H increases and the overall thermal resistance decrease with increasing H. The influence of both W and H on optimal ε is weak.

Finally, the influence of pumping power on optimal N_H and overall thermal resistance is given in Fig. 11. As the pumping power is increased, the optimal N_H increases while the overall thermal resistance decreases; meanwhile, the optimal ε decreases.

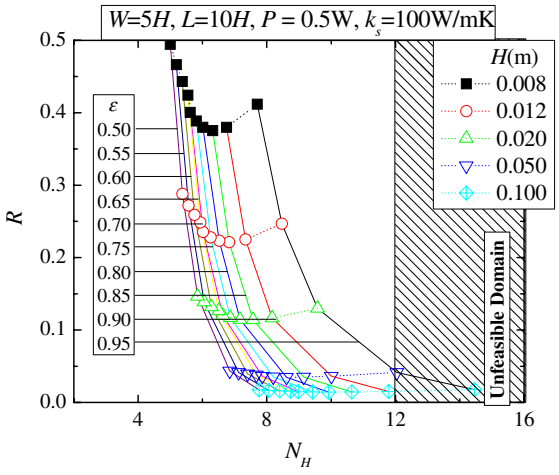

Fig. 10. Optimum cell number N_H and corresponding overall thermal resistance for square cells and selected values of heat sink height H and porosity ε, with $W = 5H$, $L = 10H$, $P = 0.5$ W and $k_s = 100$ W/m K; the working fluid is air ($Pr = 0.74$).

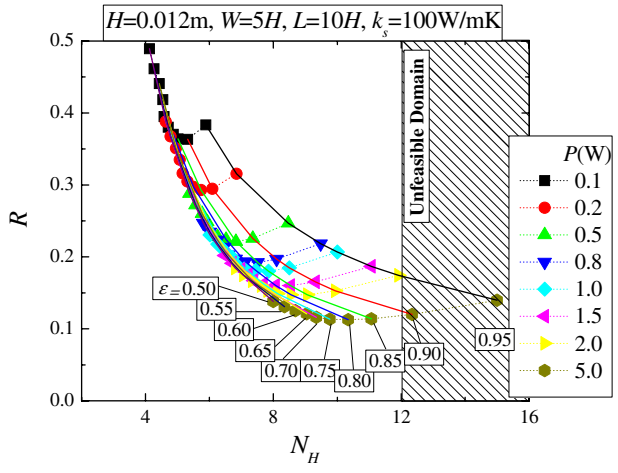

Fig. 11. Optimum cell number N_H and corresponding overall thermal resistance for square cells and selected values of pumping power and porosity ε, with $H = 0.012$ m, $W = 5H$, $L = 10H$ and $k_s = 100$ W/m K; the working fluid is air ($Pr = 0.74$).

5.3. Different fluids

In this section, water is used in lieu of air as the coolant; the properties of both are listed in Table 1. Fig. 12 plots the optimal L and overall thermal resistance as functions of cell number N_H and porosity ε for square cells, with $H = 0.012$ m, $W = 5H$, $k_s = 1000$ W/m K and $P = 0.5$ W. In comparison with Fig. 7d where all the other conditions are the same except that the coolant is air, it is found that the optimal L/H is much larger whereas the optimal N_H (ε fixed) and optimal ε (N_H fixed) are smaller; and, what's more, the overall thermal resistance is two orders smaller. The kinematic viscosity and thermal diffusivity of water are smaller than those of air, implying that the developing regimes for both velocity and thermal fields are larger in water flow, and hence the optimal heat sink length L is larger in water cooling. Furthermore, as the thermal diffusivity of water is two orders of magnitude smaller than that of air whilst its kinematic viscosity is only one order of magnitude smaller (i.e., the Pr number of water is one order of magnitude larger), the convective heat transfer coefficient directly related to the temperature gradient adjacent to cell walls is much higher in water cooling. Consequently, the comparative conductive resistance corresponding to the maximum objective function happens in a larger cell-wall thickness regime (see Section 5.1); in other words, smaller N_H for a finite ε or smaller ε for a finite N_H.

5.4. Different cell topologies

We have hereto only considered the optimization of sandwich heat sinks having square cells. To explore the influence of cell topology on the heat dissipation capability of the sandwich, in Fig. 13, the optimal geometric parameters and overall thermal resistance for equilateral triangular cells (Fig. 1d) are plotted. The working fluid is air.

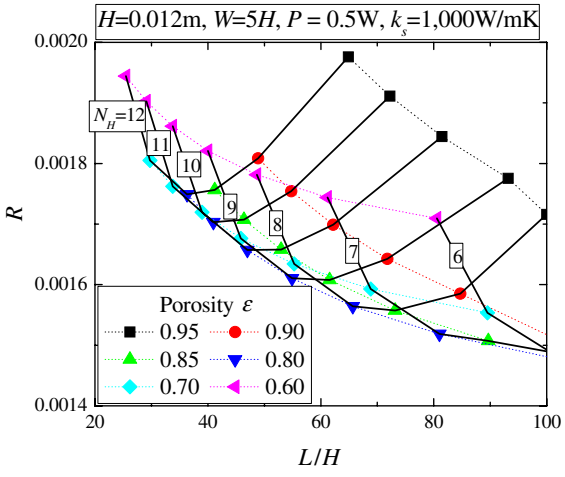

Fig. 12. Optimum heat sink length L and corresponding overall thermal resistance for square cells and selected values of cell number N_H and porosity ε, with $H = 0.012$ m, $W = 5H$, $P = 0.5$ W and $k_s = 1000$ W/m K; the working fluid is water ($Pr = 6.99$).

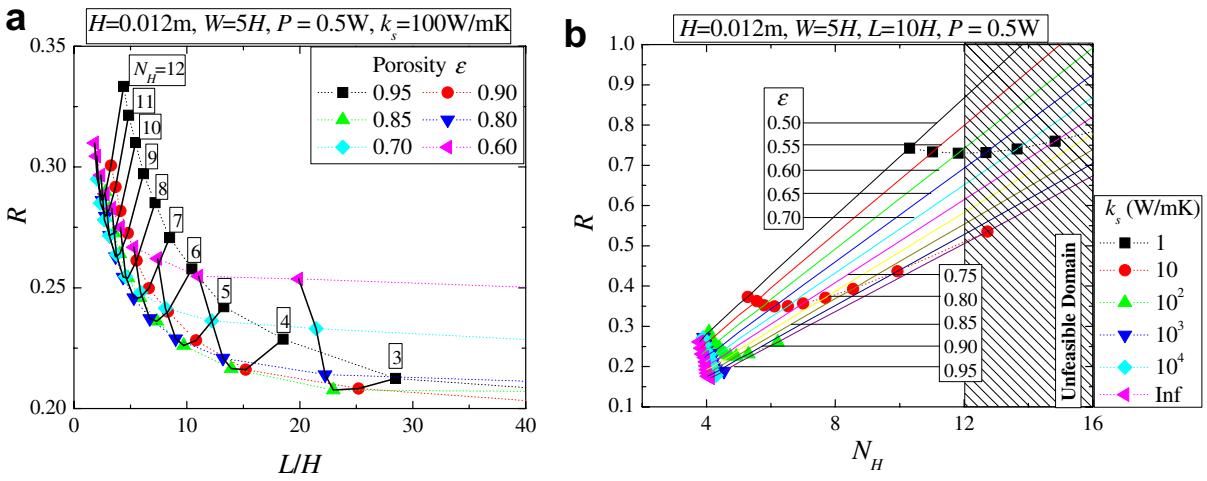

Fig. 13. (a) Optimum heat sink length L; (b) optimum cell number N_H; and corresponding overall thermal resistance for triangular cells and selected values of porosity ε and solid conductivity k_s; the working fluid is air ($Pr = 0.74$).

Comparing Fig. 13a with Fig. 7c, where all the other conditions are identical except that the cell shapes are different, we find that for 2D cellular structures having the same porosity and N_H, those with triangular cells have smaller optimal overall length than those with square cells. Similarly, comparing Figs. 13b and 11b, we find that for cellular structures having the same overall volume, those with triangular cells have smaller optimal cell number along the height than those with square cells, leading to fabrication advantages. Therefore, the results of Fig. 13a and b show cellular sandwich heat sinks with triangular cells are thermally superior. Mechanically, triangular cells also have obvious advantage over square cells, as demonstrated by Gu et al. [4].

6. Conclusions

By integrating the fin analogy model into the intersection-of-asymptotes method, the structure of a 2D cellular metallic sandwich heat sink cooled by laminar forced convection has been optimized for maximum thermal performance, subjected to fixed pumping power. CFD (FLUENT™) calculations were used to check the accuracy and reliability of theoretical model predictions. For a given pumping power and a certain Prandtl number (coolant), the heat sink has an optimal overall length if its cross-sectional topology is specified a priori, or optimal cross-sectional topology if its overall dimensions are predefined. The optimal cross-sectional topology of the heat sink is achieved when its conductive and convective thermal resistances are comparative. Various parameters that may affect the optimally designed sandwich structure were discussed, including overall structural dimensions, cell shape, pumping power, solid conductivity, and coolant properties (water versus air). Cellular sandwich heat sinks having triangular cells are found to be superior to square cells, both thermally and mechanically.

Acknowledgements

The authors wish to thank the EU HYMM project (NMP3-CT-2003-505206), the National Basic Research Program of China (2006CB601202), the National 111 Project of China (B06024), and the National Natural Science Foundation of China (10328203, 10572111 and 10632060) for partial financial support of this work.

References

[1] L.J. Gibson, M.F. Ashby, Cellular Solids: Structure and Properties, second ed., Cambridge University Press, 1997.
[2] T.J. Lu, L. Valdevit, A.G. Evans, Active cooling by metallic sandwich structures with periodic cores, Progr. Mater. Sci. 50 (2005) 789–815.
[3] T.J. Lu, Heat transfer efficiency of metal honeycombs, Int. J. Heat Mass Transfer 42 (1999) 2031–2040.
[4] S. Gu, T.J. Lu, A.G. Evans, On the design of two-dimensional cellular metals for combined heat dissipation and structural load capacity, Int. J. Heat Mass Transfer 44 (2001) 2163–2175.
[5] R.S. Kumar, D.L. McDowell, Rapid preliminary design of rectangular linear cellular alloys for maximum heat transfer, AIAA J. 42 (8) (2004) 1652–1661.
[6] C.C. Seepersad, B.M. Dempsey, J.K. Allen, F. Mistree, D.L. McDowell, Design of multifunctional honeycomb materials, AIAA J. 42 (5) (2004) 1025–1033.
[7] A. Bejan, E. Sciubba, The optimal spacing of parallel plates cooled by forced convection, Int. J. Heat Mass Transfer 35 (12) (1992) 3259–3264.
[8] A. Yilmaz, O. Buyukalaca, T. Yilmaz, Optimum shape and dimensions of ducts for convective heat transfer in laminar flow at constant wall temperature, Int. J. Heat Mass Transfer 43 (2000) 767–775.
[9] Y.S. Muzychka, Constructal design of forced convection cooled microchannel heat sinks and heat exchangers, Int. J. Heat Mass Transfer 48 (2005) 3119–3127.
[10] C.B. Williams, F. Mistree, D.W. Rosen, Investigation of solid freeform fabrication processes for the manufacture of parts with designed mesostructure, in: Proceedings of the DETC'05: ASME 2005 Design Engineering Technical Conferences and Computer and Information in Engineering Conference, Long Beach, California, USA, 2005.

[11] H.N.G. Wadley, N.A. Fleck, A.G. Evans, Fabrication and structural performance of periodic cellular metal sandwich structures, Compos. Sci. Technol. 63 (2003) 2331–2343.
[12] T. Wen, J. Tian, T.J. Lu, D.T. Queheillalt, H.N.G. Wadley, Forced convection in metallic honeycomb structures, Int. J. Heat Mass Transfer 49 (2006) 3313–3324.
[13] A. Bejan, Convection Heat Transfer, second ed., Wiley, New York, 1995.
[14] S. Mereu, E. Sciubba, A. Bejan, The optimal cooling of a stack of heat generating boards with fixed pressure drop, flowrate or pumping power, Int. J. Heat Mass Transfer 36 (1993) 3677–3686.